Constitutive models that exceed the fitting capabilities of the Herschel–Bulkley model: A case study for shear magnetorheology

Constitutive models that exceed the fitting capabilities of the Herschel-Bulkley model: A case study for shear magnetorheology

Martin Cvek

Centre of Polymer Systems, University Institute, Tomas Bata University in Zlín, Trida T. Bati 5678, 760 01, Zlín, Czech Republic

E-mail address: cvek@utb.cz

ABSTRACT

A significant proportion of non-Newtonian fluids exhibits the phenomena of shear-thinning and yield stress. The Herschel-Bulkley model is probably the most widespread equation to describe the rheological behaviour of such systems, although greater attention is being paid to discerning more accurate mathematical models for viscoplastic systems. In this regard, the work presented herein investigates existing, unconventional viscoplastic models and evaluates their fitting and predictive capabilities in relation to collected magnetorheological data. The four-parameter models of modified Carreau, modified Cross (and its variant extended with the Quemada equation), Shulman and Nasiri-Ashrafizadeh were applied to appraise the shear data of the magnetorheological fluids. Their suitability was also statistically evaluated and compared with that attained for the conventional Herschel-Bulkley model and recently employed analogues, such as the Robertson-Stiff and Mizrahi-Berk models. It was found that the performance of all models for describing magnetorheological flow curves was adequate, with relatively high correlation coefficients. Applying the four-parameter models, however, provided higher accuracy, demonstrated by notably reduced statistical coefficients of regression analysis. Both of the modified Carreau and Cross models exhibited superior fitting performance (up to 4-times lower root mean square error), while the Shulman and Nasiri-Ashrafizadeh models proved questionable in application. Although interpreting four-parameter equations is a rather complex matter, they provided more reliable prediction of shear stress data across the entire range of shear rate than the Herschel-Bulkley approximation, especially the modified Carreau and modified Cross models. It is believed that these findings can be extended to describe the rheology of other systems with viscoplastic characteristics.

Keywords: Modelling, viscoplasticity, rheology, yield stress, herschel-bulkley, cross model, carreau model

1. Introduction

An advanced technique for exploiting the capabilities of the various materials is contactless management of their properties. Recent decades have witnessed the proposal of a plethora of systems driven by magnetic or electric fields, UV light and so on, yet these are still undergoing technological development and modification. Research on magnetorheological (MR) suspensions commenced in the late 1940s (**Rabinow**, **1948**), although the first commercial application (**Wollny et al.**, **2001**) was not until 2002, in shock absorbers by the Delphi Corporation fitted to the Cadillac Seville STS car. Such delay in progress, particularly for these systems, was caused by the poor quality of MR suspensions and related technical issues, e.g. the need for heavy, bulky electromagnets (**Tao**, **2001**). A period of intense investigation has since led to MR formulations being fabricated, the construction of

engineering prototypes and diversification in the marketplace for MR suspensions, for example, in the automotive sector, robotics and civil engineering (**de Vicente et al.**, **2011**; **Kuzhir et al.**, **2005**).

The MR suspensions are classified as mixtures of magnetically permeable microparticles dispersed in a low-viscosity, non-magnetic carrier fluid. They constitute non-Newtonian fluids capable of producing rapid and reversible changes in their rheological properties in reaction to an externally applied magnetic field. These changes stem from field-induced particle reorganization, i.e. alteration from a random to a highly organized state (**Cvek et al.**, **2016**). Compared to the other viscoplastic materials that are characterized in the Couette geometry (**Skadsem** and **Saasen**, **2019**), the rheology of the MR suspensions is mostly studied using the parallel-plate (PP) or the cone-plate (CP) geometries. Such configurations allow to induce the particle structures in a preferential direction (perpendicular to the plate) to achieve the maximum effects of the field. The CP offers the constant shear rate inside the sample volume, but its variable gap induces the particle architectures with a variable length of the aggregates. On the contrary, the shear rate in the PP geometry is not constant, but it produces more uniform aggregates and allows the adjustment of the upper-plate to avoid slipping phenomenon, which makes the PP geometry to be the most widely used for magnetorheology (**Bossis et al.**, **2002b**). To ensure the magnetic field inside the geometry, in the early works, a toroidal coil was placed around a sample cell, i.e. the Helmholtz configuration (**Volkova et al.**, **1999**). A later innovation was the introduction of a commercial rheometer incorporating a coil (**Laun et al.**, **2011**; **Wollny et al.**, **2001**). A common method for characterizing MR suspensions is to conduct a shear rotational test, which gives a corresponding flow curve, typically containing the yield stress and pseudoplasticity patterns.

The yield stress is referred to as the most relevant parameter for the MR suspensions, and is considered as a proxy of their efficiency (**Bossis et al.**, **2002**b). In magnetorheology, different yield stresses can be distinguished; the "apparent" yield stress is typically called the dynamic yield stress, while a "true" yield stress is referred to as the static (or frictional) yield stress. While the former corresponds to the continuous disruption of the particle chains during the low shear limit, the latter one is attributed to a sudden collapse of the structure, or the slippage of the aggregates on the plates. It is noteworthy that the dynamic yield stress can be obtained indirectly by fitting the controlled shear rate (CSR) data and extrapolating them to the zero-shear rate, and, the static yield stress is obtained from the controlled shear stress (CSS) data, deduced from the stress threshold associated with the sudden drop in viscosity (**de Vicente et al.**, **2011**).

Constitutive modelling is considered an effective mathematical tool for describing rheological data in just a few parameters, preferably relating to a physical property. The parameters extracted can pertain to physical quantities, which serve to compare a series of specimens qualitatively. As mentioned, the efficiency of MR suspensions is determined by the corresponding value for the dynamic yield stress (a fitting parameter), constituting the maximum stress that a suspension withstands before flow commences (**Bossis et al.**, **2002a**). For this procedure, several viscoplastic models have been applied with varying degrees of success (see **Table 1**). It should be noted that empirical fitting models merely represent a simplified, albeit essential, description of the flow behaviour of a material (**Pivokonsky** and **Filip**, **2014**).

The Bingham Plastic (BP) model (**Eq**. (**1**)) has gained in popularity, predominantly due to its simplicity, although it does not fully correspond with the physical reality of MR suspensions (**Kelessidis** and **Maglione**, **2006**). This model compartmentalizes the complex behaviour of viscoelastic matter to a response that is purely elastic (pre-yield stress) and viscous (post-yield stress), thus it predicts constant viscosity once yield stress is exceeded. As the aspect of fitting is absent in the nonlinear portion of the flow curve, BP model is considered to be the least suitable equation for fitting rheological data, compared to other analytical models. Since pseudoplasticity is a typical phenomenon occurring in the

MR suspensions (especially in the presence of a magnetic field), BP model serves only as an approximate gauge of yield stress (**Bossis et al.**, **2002a**). To avoid discontinuity in the flow curve that causes a series of difficulties in the analytical or even numerical calculations, the BP model was smoothened using the $1 - \exp(-x)$ function by Papanasta-siou (**Eq**. (**2**)) addressing the both, pre-yield and post-yield regions (**Papanastasiou**, **1987**; **Susan-Resiga**, **2009**). The drawback of the BP model is also eliminated by the Herschel-Bulkley (HB) equation (**Eq.** (**3**)) that introduces the power-law exponent, n, which takes into the account the nonlinear character of the flow curve; for pseudoplastic (shear thinning) materials $n < 1$, for dilatant materials (shear thickening) $n > 1$, while for Newtonian liquids $n = 1$, and HB model reduces to the BP model. The HB model is the more suitable variant as a consequence, in addition to being the most commonly applied viscoplastic model for shear-thinning materials. Its applicability for predicting the flow behaviour of MR suspensions has recently been questioned, however, as it appears to under- and overestimate apparent shear stress values in the lower and higher regions of shear rate, respectively (**Cvek et al.**, **2016**).

Table 1 Overview of the viscoplastic rheological models.

Model equation	Model title (model ID)	Number of fitting parameters	Appearance in magnetorheology	Eq.
$\tau = \tau_0 + \eta_P \dot{\gamma}$	Bingham plastic (BP) model	2P	(Bahiuddin et al., 2018b; Esmaeilnezhad et al., 2017; Gao et al., 2017) besides others.	(1)
$\tau = \left[\eta_0 + \frac{1-\exp(-n\lvert\dot{\gamma}\rvert)}{\lvert\dot{\gamma}\rvert}\right]\dot{\gamma}$	Papanastasiou model	2P	(Bahiuddin et al., 2019; Daniel et al., 2014; Elsaady et al., 2020; Farjoud et al., 2011; Susan-Resiga, 2009)	(2)
$\tau = \tau_0 + K\dot{\gamma}^n$	Herschel-Bulkley (HB) model	3P	(Bahiuddin et al., 2018a, 2018b; Esmaeilnezhad et al., 2017; Gao et al., 2017; Min et al., 2017; Romano et al., 2017) besides others.	(3)
$\tau = \left[K^{\frac{1}{n}}\lvert\dot{\gamma}\rvert^{\frac{n-1}{n}} + \left(\frac{\tau_0}{\lvert\dot{\gamma}\rvert}\right)^{\frac{1}{n}}\right]^n \dot{\gamma}$	Robertson-Stiff (RS) (Vocadlo) model	3P	(Bahiuddin et al., 2018b; Cvek et al., 2021; Cvek et al., 2018; Cvek et al., 2016; Cvek et al., 2020; Min et al., 2017; Ronzova et al., 2021; Plachy et al., 2018)	(4)
$\frac{1}{\tau^2} = \frac{1}{\tau_0^2} + K\dot{\gamma}^n$	Mizrahi-Berk (MB) model	3P	(Cvek et al., 2016; Min et al., 2017; Romano et al., 2017)	(5)
$\eta = \tau_0\dot{\gamma}^{-1} + \eta_\infty[1 + (\lambda\dot{\gamma})^2]^{-N}$	modified Carreau (mCA) model[a]	4P	This paper	(6a)
$\tau = \{\tau_0\dot{\gamma}^{-1} + \eta_\infty[1 + (\lambda\dot{\gamma})^2]^{-N}\}\dot{\gamma}$				(6b)
$\eta = \tau_0\dot{\gamma}^{-1} + \eta_P(1 + \alpha\dot{\gamma})^{-m}$	modified Cross (mCR) model[a]	4P	This paper	(7a)
$\tau = \tau_0 + [\eta_P(1 + \alpha\dot{\gamma})^{-m}]\dot{\gamma}$				(7b)
$\eta_\infty = \eta_F\left(1 - \frac{\varphi}{\varphi_M}\right)^{-2}$	Quemada equation	Not applicable	(Ruiz-Lopez et al., 2016, 2017) besides others.	(8)
$\eta = \tau_0\dot{\gamma}^{-1} + \frac{\eta_0 - \eta_\infty}{1 + (\alpha\dot{\gamma})^m} + \eta_\infty$	modified Cross model and its version extended with Quemada equation (Ex-mCR)	4P	This paper	(9a)
$\tau = \tau_0 + \frac{\eta_0 - \eta_\infty}{1 + (\alpha\dot{\gamma})^m}\dot{\gamma} + \eta_\infty\dot{\gamma}$				(9b)
$\tau = \tau_0 + \frac{\eta_0 - \eta_F\left(1 - \frac{\varphi}{\varphi_M}\right)^{-2}}{1 + (\alpha\dot{\gamma})^m}\dot{\gamma} + \dot{\gamma}\eta_F\left(1 - \frac{\varphi}{\varphi_M}\right)^{-2}$				(9c)
$\tau = \left[K^{\frac{1}{m}}\lvert\dot{\gamma}\rvert^{\frac{1}{m}-\frac{1}{n}} + \left(\frac{\tau_0}{\lvert\dot{\gamma}\rvert}\right)^{\frac{1}{n}}\right]^n \dot{\gamma}$	Shulman (SM) model	4P	This paper	(10)
$\tau = \tau_0 + b\dot{\gamma} + k\dot{\gamma}^{n-m}\ln(1 + \dot{\gamma})$	Nasiri-Ashrafizadeh (NA) model	4P	This paper	(11)

[a]*The mathematical structure and designation of all the quantities in the presented models were adopted from the original publications (slightly different variations of the quoted models can be found in the literature).*

To address this issue, we recently analysed the predictive and fitting capabilities of 3-parameter ($3P$) viscoplastic models typically used in other areas of research, subsequently augmenting the field of shear magnetorheology with the Robertson-Stiff (RS) and Mizrahi-Berk (MB) models (**Eq. 4**, and **5**). It was concluded that RS model exhibited a superior, close fit to the experimental data in comparison

with HB model, whereas the prediction by MB model appeared to be the least suitable (**Cvek et al.**, **2016**). Other researchers however reported different observations (**Min et al.**, **2017**). For their systems (**Min et al.**, **2017**), the MB model provided the greatest accuracy as regards fitting, while RS model possessed the best fit solely in situations where the magnetic field was of high strength. As described later herein, resolving this inconsistency is closely linked to the primary objectives of this manuscript.

It is clear that analysis of rheological behaviour is a crucial procedure during the design of MR devices (**Bahiuddin et al.**, **2018a**). As the flexibility of $3P$ models is considered somewhat limited, an attempt was made herein to employ viscoplastic models with four fitting parameters ($4P$) in order to provide more reliable, robust description of MR data. The 4P models suggested to date in the literature have not been tested across magnetorheology. In addition to MR fluids, non-Newtonian systems exist in abundance in nature (**Khan et al.**, **2018**), hence phenomena connected to non-Newtonian flows have been variously investigated, for example, in mining in relation to slurry and mud (**Kelessidis** and **Maglione**, **2006**), in the foodstuffs (**Pelegrine et al.**, **2002**), pharmaceutical and cosmetics sectors (**Song et al.**, **2006**), and the biomedical sphere, i.e. in blood flow (**Apostolidis** and **Beris**, **2014**). Furthermore, it is a commonplace occurrence in industry to process polymers in a molten state that typically exhibit non-Newtonian traits. When filled with solids, they even exhibit yield stress after exceeding a certain concentration, as forces of particle interaction rise to a significant level, in a similar manner to MR fluids.

From the perspective of mathematics, the rheological behaviour of glass-filled polymers has been successfully described by the Carreau model (**Poslinski et al.**, **1988**) with the integrated yield stress term. In order to derive the modified Carreau model (mCA; **Eq.** (**6**)), the power-law dependence in the HB model has to be substituted by the Bird-Carreau expression, as demonstrated by (**Poslinski et al.**, **1988**). Having one additional parameter makes the mCA model suitable for evaluating the flow of MR suspensions. The Cross model is a widely applied rheological equation typically used to gauge the flow behaviour of various food products, including solutions of xanthan gum, guar gum (**Rayment et al.**, **2000**) and starch (**Rayment et al.**, **1995**). It has also been shown to predict the viscosity of synthetic polymers and related mixtures (**Mannarswamy et al.**, **2010**). In a paper by (**Rayment et al.**, **2000**), the Cross model was modified to include a parameter for yield stress, giving rise to a modified viscoplastic equation (mCR; **Eq.** (**7**)). The modified Cross model inclusive of a yield stress was also used by (**Pease et al.**, **2019**) to predict behaviour of the radioactive Hanford slurry. Some variants of the mCR model (Rayment et al., 2000) can be further extended by the Quemada equation, which was originally developed for blood rheology (**Quemada**, **1998**), and later successfully applied for rheological modelling of cementitious materials (**Hodne et al.**, **2007**) and drilling fluids (**Baldino et al.**, **2018**), despite its limited applicability in the presence of non-zero yield stress (**Knutsen et al.**, **2021**). In magnetorheology, the phenomenological Quemada equation (**Eq.** (**8**)) is usually used to estimate the limiting, i.e. high-shear, viscosity of the MR suspensions, under the assumption of a random close packing for the spheres (**Ruiz-Lopez et al.**, **2016**). To this date, the mCR extended with the Quemada (Ex-mCR) model (**Eq.** (**9**c)) has not been tested to describe the MR shear data. Further, a very rare empirical constitutive model for viscoplastic materials was reported by (**Gorislavec et al.**, **1968**), wherein their $4P$ model could be perceived as an extension of the RS equation having one additional fitting parameter. This particular expression is attributed to the renowned rheologist Zinovii Shulman (deceased 2007), though the Shulman (SM) model as it is known (**Eq.** (**10**)) has not entered into common usage. Finally, a hybrid equation of the BP, power-law and the HB models with a logarithmic correction factor was developed by (**Nasiri** and **Ashrafizadeh**, **2010**) to predict the rheological parameters of the drilling fluids in an annulus (**Eq.** (**11**)). The model was originally termed as the New Equation, however, it found its way to a broader audience (**Andaverde et al.**, **2019**; **Mohamed et al.**, **2021**); thus, it was herein abbreviated as the "NA model". The aim of this paper is to refine and

compare the predictive and fitting capabilities of the referred $3P$ and $4P$ models by evaluating the MR steady shear data.

The following nomenclature was applied In the rheological models (**Table 1**): τ is shear stress, τ_0 stands for dynamic yield stress, $\dot{\gamma}$ is the shear rate, K equals the consistency index, η represents the apparent viscosity, η_P (analogy with b parameter in the NA model), η_0 and η_∞ are the plastic, zero-shear and infinite-shear rate viscosities of the suspension, respectively; η_F denotes the viscosity of the carrier liquid, n is the power-law index, λ and α are time constants related to the relaxation time, while m and N are dimensionless exponents. The symbols φ and φ_M represent the actual particle volume fraction, and maximum packing fraction, respectively, while the latter accounts for 0.64 for the random close packing fraction of spheres (**Ruiz-Lopez et al.**, **2017**). Furthermore, it is important to emphasize that the NA model incorporates only 4 independent parameters, since the term $(n - m)$ is considered as a single parameter (**Nasiri** and **Ashrafizadeh**, **2010**). The validity of the NA equation is restricted to the following conditions: $0 = n \leq 1$, $0 = m \leq 1$, and $b \geq 0$, while the value of $(n - m)$ was reported to be rarely less than zero for the best fit (**Nasiri** and **Ashrafizadeh**, **2010**).

Upon a review of the literature referenced, it become clear that it was necessary to refine the conventional fitting procedure of data on MR steady shear by looking at models from other fields of research, and the findings of this study are given herein. The 4P viscoplastic models, namely mCA, mCR, Ex-mCR, SM and NA, were employed so as to describe MR data, in addition to which their fitting and predictive applicability was statistically investigated and compared to that of conventional 3P analogues, i.e. HB, RS and MB models. In order to raise the level of relevancy from a practical perspective, a representative MR fluid was designed that had virtually the same solid content as commercial products(**Datasheet; Datasheet**). Besides that, the robustness and fitting generality of the models was considered by evaluating the resultant MR data, recorded under different settings on a rheometer. Thus, the next objective was to explore whether the performance of the models was restricted to the measuring protocol, this constituting an adjustable input by the operator.

2. Experimental part

2.1. Materials

The material used to obtain the representative flow curves was an MR suspension based on silicone oil (Lukosiol, Chemical Works, Czech Republic) and carbonyl iron (CI) micropowder (SL grade, BASF, Germany). According to the producers, the oil has a density of 0.97 g/cm^3 and dynamic viscosity of 197 mPa s at 25 °C; while the CI particles possessed a density of 7.79 g/cm^3 and diameters ranging between 1 and 5 µm. The MR suspension possessed a solid content of 75 wt% (27.2 vol %), as is typical for commercial products (Datasheet; Datasheet), and was carefully homogenized prior to use. During the process, thorough mechanical stirring occurred, followed by sonication on an ultrasonic processor (UP400S, Hielscher Technologies, Germany), equipped with a titanium sonotrode ($H7$), under the desired conditions (an acoustic power density of 300 W, working frequency of 24 kHz and pulse mode factor of 80%). The overview of the research protocol is shown in **Fig. 1**.

2.2. Rheological data

Rheological data was gathered on a rotational rheometer (Physica MCR 502, Anton Paar, Austria), set up with a magneto cell (MRD170/ 1T) and parallel-plate (PP20/MRD/TI) geometry with a constant gap of 0.5 mm. The magnetic field perpendicular to the plates was provided by an external power source (PS/MRD/5A), supplying electromagnetic coils located beneath the sample cell. The sample was well

dispersed and carefully dosed between the plates prior to testing. Before each experiment, the usual steady pre-shear (100 s^{-1}, 60 s) step was carried out to ensure initial conditions remained identical. Shear rates from 0.01 to 500 s^{-1} with logarithmic scaling (6 pts. Per decade) were subsequently applied in the off-state, and under various magnetic field strengths of up to 360 kA m^{-1} (at an increment of 72 kA m^{-1}).

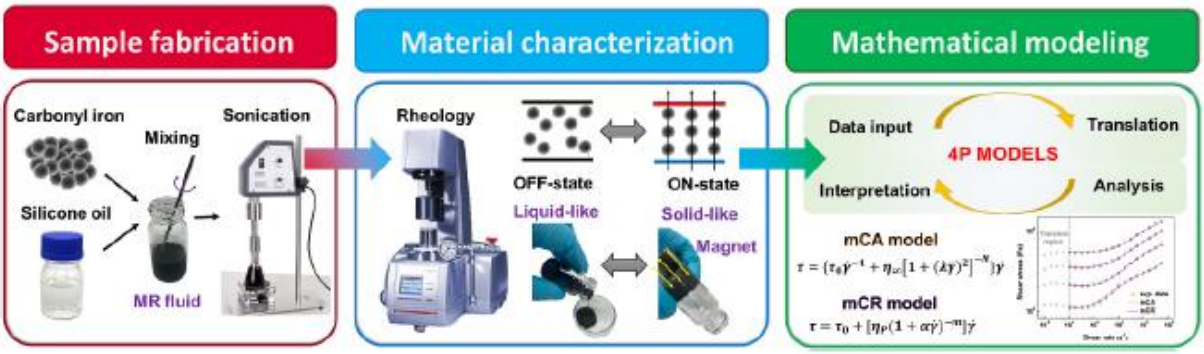

Fig. 1. The simplified overview of the research protocol.

This ensured reasonable homogeneity of the magnetic field, which would otherwise (at higher fields) have transformed into an M-shape profile along the rheometer plate with a saddle point on the rotation axis, provoking the outward migration of particles under magnetic field gradients. Each data point was taken at a constant time interval, Δt = 10 s, meaning the experiment lasted a total of 500 s. The vast majority of the MR research does not refer to the time interval is not mentioned of such tests, although recent works (**de Vicente** and **Berli**, **2013**) indicate that At as selected permits reasonable latency for gathering data, even though some complex fluids may require more time to reach a steady state. Extending the duration of the experiment could have resulted in the particles settling, and the given experimental conditions were considered the most favourable. Prior to taking each on-state measurement, the corresponding magnetic field was applied (60 s) under static conditions to equilibrate the suspension by developing the columnar structures inside the geometry (**Wang et al.**, **2014**). The normal force increased as a result, indicating a better contact between the particle columns and upper plate geometry (**Cvek et al.**, **2016**). Despite that, the possibility of the wall slip could not be ruled out, since the upper plate had not been sandblasted. The desired temperature (25 °C) in the sample cell was kept constant with the aid of a thermostatic device (Julabo FS18, Germany). The flow curves were collected three times to ensure reproducibility, and mean values were applied for constitutive modelling.

The start-up experiment was conducted in accordance with a protocol, as follows: the fresh MR suspension was pre-sheared (100 s^{-1}, 60 s), equilibrated under static conditions (at the given magnetic field, 60 s) and a constant shear rate (0.4, 1.0 or 4.0 s^{-1}) was imposed for a long duration (>400 s). Data were collected at constant intervals, $\Delta t = 0.5$ s, a time selected to acquire the dynamics of the start-up response, specifically initial transient effects (**Carrier** and **Petekidis**, **2009**).

2.3. Data processing

The experimental data gathered was fitted by the given viscoplastic models (**Table 1**) and the quality of such fitting numerically evaluated (**Table 2**, **Eq.** (**12**)-(**14**)). Since evaluation with the correlation coefficient R^2 is not completely relevant for nonlinear models, the sum of square errors (SSE) and root mean square errors ($RMSE$) were applied as more reliable statistical parameters for describing the close fitting of the models (**Kelessidis** and **Maglione**, **2006**).

The R^2 is given by **Eq. 12**, where t is the observed shear stress, τ_p the predicted shear stress, Tmean the mean shear stress and N the number of measurements.

Table 2 Formulas for calculation of statistical indicators.

$$R^2 = 1 - \frac{\sum_i^N (\tau_i - \tau_p)^2}{\sum_i^N (\tau_i - \tau_{mean})^2} \quad (12)$$

$$SSE = \sum_i^N (\tau_i - \tau_p)^2 \quad (13)$$

$$RMSE = \sqrt{\frac{SSE}{N-p}} \quad (14)$$

For the SSE and $RMSE$ calculated by **Eq. 13** and **Eq. 14**, respectively, the parameters are defined as above, and p denotes the degrees of freedom (expressed as the number of parameters) of the particular model. Higher values for R^2 and lower ones for SSE and $RMSE$ clearly relate to minor discrepancies between the measured and predicted shear stress data. Note that R^2 ranges from 0 to 1, while $R^2 \geq 0.8$ conventionally represents a strong correlation, $0.2 < R^2 < 0.8$ denotes a correlation and $0.2 \leq R^2$ suggests a weak correlation (**Gullu**, **2016**).

3. Results and discussion

3.1. Interpretation of MR data with respect to model formulations

In order to collect representative experimental data, the MR fluid was subjected to typical shear MR conditions. As per the solid content present, the MR fluid resembled commercial products in composition (Datasheet; Datasheet). The suspension exhibited almost Newtonian behaviour in the absence of a magnetic field, whereas imposing one exerted a dramatic increase in shear stress accompanied by the appearance of τ_0 and a nonlinear response; effects typical of an MR suspension, as variously published in the literature (**de Vicente et al.**, **2011**). Such behaviour stems from interplay between the structure built up and its subsequent breakdown, which is dependent on the rate of shearing, strength of the magnetic field, composition of the MR suspensions, duration of the shearing cycle and so on.

As for other complex materials (**Divoux et al.**, **2011**), MR fluids can exhibit transient dynamics, such as a non-monotonous rheological response (**de Vicente** and **Berli**, **2013**), herein detected in a low γ region (**Fig. 2**). The transient state generally exhibited initial rise in τ, the maximum value corresponding to static (frictional) yield stress, followed by a drop in stress towards a steady state (**Barnes**, **1999**). For better comprehension of the transient behaviour, start-up shear experiments at various levels of $\dot{\gamma}$ were conducted. **Fig. S1** clearly shows a strong increase in the τ that appeared when shearing took place at low γ, a phenomenon caused by the particle chains deforming elastically, and these continuously breaking chains were able to develop new structures (**Jonkkari** and **Syrjala**, **2011**). When exposed to a greater level of $\dot{\gamma}$ in the start-up shear test, the deformation mechanism changed, since

the particle chains broke rapidly and any new structures had insufficient time to recover, a finding which correlated with results reported elsewhere (**Jonkkari** and **Syrjala**, **2011**; **Ulicny et al.**, **2005**). Although a faster relaxation stage after the stress overshoot was detected under a low magnetic field (**Fig. S1a**), compared to high magnetic field (**Fig. S1c**), it became clear that the time required to reach the steady state in the MR fluids was much longer than $\geq 3/\dot{y}$, which is a criterion typically reported for other forms of complex fluid (**Divoux et al.**, **2016**).

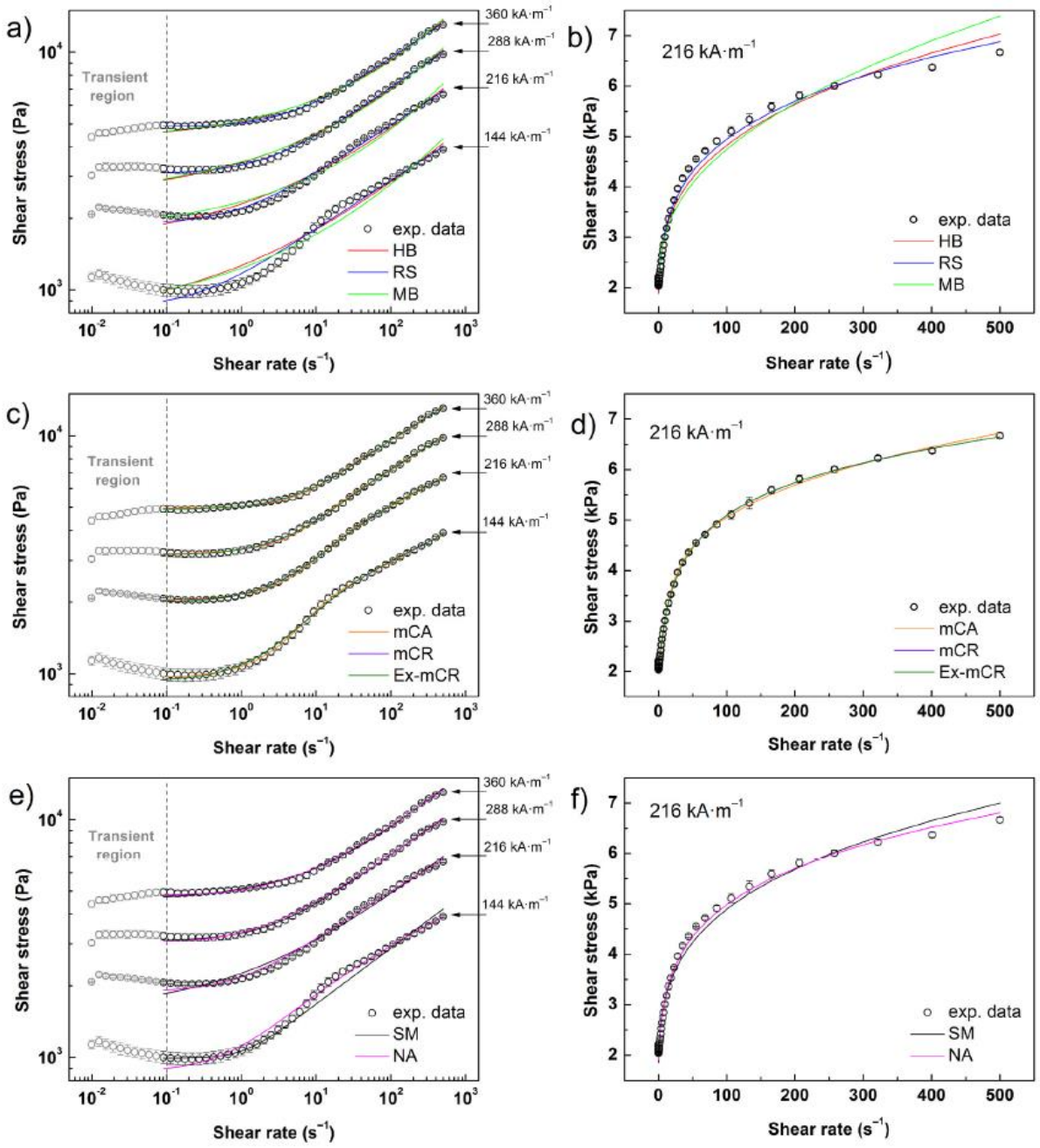

Fig. 2. Shear stress plotted against shear rate for the MR fluid (50 pts., $\Delta\tau = 10$ s) under various magnetic field strengths; the data was fitted by $3P$ models (a, b), and $4P$ models (c-f).

The existence of a transient rheological response was considered when coordinating the methodology for constitutive modelling. Since the applied $3P/4P$ viscoplastic models were represented mostly by monotonic equations, only the relevant part of each flow curve, i.e. the steady state, was subjected to the fitting procedure. Since the transient state was generally limited to $\dot{y}$ 10^{-1} s^{-1}, and as majority of MR devices operate at much greater shear rates (**Roupec et al.**, **2020**), any existence of a transient state was further disregarded, upon its exclusion from the fitting procedure.

Before entering into interpretation of the data, it is necessary to discuss the difference between the RS and MB models, in light of the inconsistency between the fitting results of papers (**Cvek et al.**, **2016**) and (**Min et al.**, **2017**). In the RS model (**Eq.** (**4**)), the τ_0 parameter does not represent such a strict singularity as additive member τ_0 in the latter one (**Eq.** (**5**)). Therefore, the RS model is likely to correspond better with reality (**David et al.**, **2013**a), which explains its superior fitting capability. The course of shear stress in paper by (**Min et al.**, **2017**) exhibited an out-of-trend overshoot (see **Fig. 7**b therein), though; this potentially indicated the onset of flow instabilities (**Volkova et al.**, **1999**), such as inward/onward particle migration in the PP geometry (**Jonkkari** and **Syrjala**, **2011**). As a consequence of local maximum appearance (at a relatively high level of $\dot{y}$), the fitting capabilities of both models was considered distorted and no clear conclusion could be drawn. Admittedly, differences may also have stemmed from factors relating to composition, e.g. oil viscosity, dimension/size distribution of the particles and the volume fraction, or those pertaining to methodology, such as the upper-plate material or texture and gap height (**Jonkkari et al.**, **2012**). These inconsistencies also justified the necessity to refine the fitting procedure for the MR data.

The raw data was described by 3P models firstly; the parameters gauged are detailed in the electronic supplementary material (**Table S1**). Although the MR fluid and experimental conditions herein differed slightly from a previous study (**Cvek et al.**, **2016**), similar conclusions could still be drawn. The RS model proved to be the most suitable of the $3P$ models, thus it was employed as a reference to assess the fitting capabilities of the newly implemented $4P$ models. The accuracy of any model in describing experimental data depends on its ability to fit the nonlinear portion at relatively low γ (**Gullu**, **2016**). The flexibility of the model as to how it bends is also relevant to high shear rates, especially for strongly pseudoplastic materials ($n \ll 1$). **Fig. 2** shows the representative MR flow curves; for better depiction of differences in fitting accuracy, the representative situation in linear scales is plotted as well. As depicted in **Fig. 2**b, the HB and MB models tend to under- and overestimate shear stress values at lower or higher ranges of shear rate. Applying RS model resulted in relatively accurate fitting, though room for the improvement existed, as addressed in this study. **Fig. 2**c-f shows the fitting capabilities of the newly introduced $4P$ models, and their parameters are summarized in **Table 3**. The $4P$ models generally provided acceptable or even superior fitting capability over their $3P$ analogues, hence the $4P$ models were considered the more desirable option for parametric fitting, as elaborated later in text.

3.2. Qualitative analysis, model parameters

The flow behaviour of the MR suspensions was translated into corresponding model constants to conduct qualitative analysis. Regarding the rheology of the MR fluids, the most relevant parameter was yield stress, τ_0, referred to as “dynamic” when obtained from the viscoplastic models applied on the CSR data. Dynamic τ_0 is associated with continuous disruption of aggregates during flow, following the polarization model and the involvement of certain regimes (**Ginder et al.**, **1996**). Under the action

of a low magnetic field, dynamic τ_0 exhibits quadratic growth ($\propto H^2$), while at higher fields local saturation magnetization constitutes a factor, and dynamic τ_0 scales in adherence with $\propto H^{3/2}$.

Table 3 Numerical fitting results for the implemented $4P$ models (50 pts., $\Delta\tau = 10$ s).

Model ID	Magnetic field (kA/m)	τ_0 (Pa)	η_∞ (Pa·s)	N (−)	λ (s)	R^2 (−)	SSE ($Pa^2 \times 10^3$)	RMSE (Pa)
mCA	0	7.289	1.585	0.020	1.199	0.9998	0.138	1.730
	72	362.6	130.6	0.327	0.842	0.9964	35.90	27.94
	144	959.5	115.2	0.381	0.100	0.9998	8.69	13.75
	216	2033	113.9	0.367	0.060	0.9997	59.27	32.90
	288	3191	133.8	0.336	0.058	0.9993	253.2	71.51
	360	4944	121.6	0.319	0.045	0.9995	261.1	75.35

Model ID	Magnetic field (kA/m)	τ_0 (Pa)	η_p (Pa·s)	m (−)	α (s)	R^2 (−)	SSE ($Pa^2 \times 10^3$)	RMSE (Pa)
mCR	0	7.281	1.761	0.040	16.17	0.9998	0.138	1.734
	72	345.7	310.5	0.667	2.723	0.9954	44.97	31.27
	144	931.2	175.5	0.810	0.133	0.9993	31.49	23.46
	216	1998	162.2	0.800	0.069	0.9996	42.50	36.12
	288	3155	184.1	0.733	0.067	0.9996	108.6	48.58
	360	4908	161.8	0.707	0.048	0.9996	184.4	63.33

Model ID	Magnetic field (kA/m)	τ_0 (Pa)	η_0 (Pa·s)	m (−)	α (s)	R^2 (−)	SSE ($Pa^2 \times 10^3$)	RMSE (Pa)
Ex-mCR	0	7.264	3.535	0.099	1037	0.9998	0.139	1.734
	72	307.9	689.9	0.756	4.280	0.9968	20.49	21.10
	144	928.7	185.8	0.879	0.112	0.9964	48.15	32.35
	216	1993	175.5	0.865	0.060	0.9978	25.61	23.59
	288	3144	212.0	0.798	0.061	0.9947	104.8	47.73
	360	4895	186.9	0.781	0.041	0.9998	187.2	63.79

Model ID	Magnetic field (kA/m)	τ_0 (Pa)	K (Pa·s)	n (−)	m (−)	R^2 (−)	SSE ($Pa^2 \times 10^3$)	RMSE (Pa)
SM	0	8.707	2.092	0.093	0.101	0.9996	0.634	3.712
	72	323.6	0.031	4.157	4.153	0.9937	65.16	37.64
	144	991.4	4.89×10^{12}	0.113	0.482	0.9917	705.3	123.8
	216	1593	3.96×10^{12}	0.584	2.335	0.9948	912.2	140.8
	288	3093	4.23×10^{14}	0.255	1.100	0.9987	450.7	99.00
	360	4596	3.49×10^{12}	0.466	1.728	0.9981	962.4	144.6

Model ID	Magnetic field (kA/m)	τ_0 (Pa)	b (Pa·s)	k (Pa·s)	n (−) m (−)	R^2 (−)	SSE ($Pa^2 \times 10^3$)	RMSE (Pa)
NA model	0	5.573	1.205	2.407	0.508 0.509	0.9998	0.133	1.702
	72	331.9	1.574	201.5	0.475 0.592	0.9994	5.327	10.76
	144	870.2	<0.001	358.0	0.510 0.461	0.9978	151.8	57.44
	216	1887	<0.001	417.7	0.439 0.336	0.9981	337.5	85.65
	288	3045	<0.001	431.6	0.578 0.423	0.9989	390.3	92.12
	360	4788	<0.001	393.5	0.609 0.406	0.9987	666.4	120.4

Upon reaching the point of saturation magnetization, dynamic τ_0 is no longer dependent on the magnetic field applied. As detailed in **Fig. 3**, the fitting results partially followed the theoretical estimation given, however, dynamic τ_0 scaled with a slope close-to 1.5 across the entire range of strength of the magnetic field, regardless of the model employed. The existence of such a single-state regime had been observed previously for low-to-moderately filled MR suspensions (**Cvek et al.**, **2020**; **Esmaeil-nezhad et al.**, **2017**), which were easily susceptible to be magnetized. In relation to parametric

modelling, **Fig. 3** shows that all the models predicted comparable dynamic t0 values. The slope of the extracted dependences ranged from 1.58 to 1.68 for the $3P$ models, and from 1.62 to 1.72 for the $4P$ models. The RS model, and its $4P$ counterparts, denoted as mCA, mCR (and Ex-mCR; for $H \geq 144$ kA m^{-1}), exhibited noticeably similar τ_0 predictions with variance of less than 5% in absolute values. For all models under the investigation, differences in τ_0 values were below 15% in the majority of cases (**Table 3**). In summary, variation in the τ_0 predicted by the $3P$ and $4P$ models was rather marginal, though the actual values did not necessarily correspond with their fitting capability (as discussed later).

Examining variance in the parameter K between the $3P$ models revealed that such values for the HB and MB models increased in line with magnetic field strength (**Table S1**). Different trends were observed for n values, however, where n was virtually equal to 1 in the absence of a magnetic field, suggesting near Newtonian behaviour; this was followed by a significant drop to 0.35 and 0.21, respectively, when the field was applied. In the RS model, the on-state value n remained almost constant, while for HB model n rose in opposition to the nonlinearity of the flow curves. The almost constant values for n were also experimentally found for the suspensions upon introduction of glass spheres or glass fibres (**Poslinski et al., 1988**). In light of this evidence, the HB model demonstrated less capability to adjust any nonlinearity compared to the RS one. This finding is consistent with that obtained for jet grouting cement mixtures with similar types of flow curve (**Gullu, 2016**). The parameters K and n changed arbitrarily in the case of the MB model, thus the meaning of their physical is rather speculative.

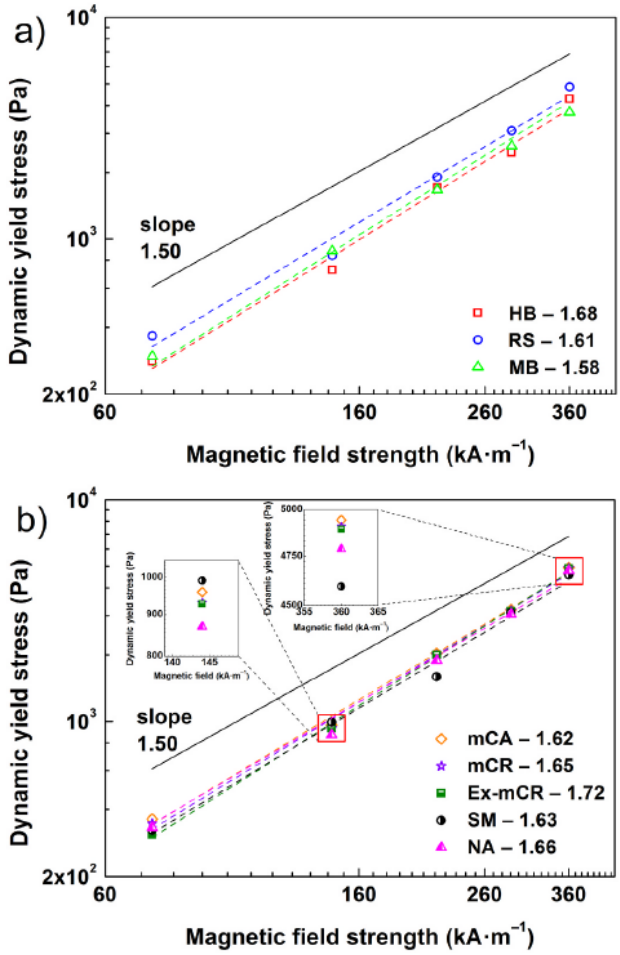

Fig. 3. Dynamic τ_0 obtained from the $3P$ (a) and $4P$ models (b), plotted against magnetic field strength for the representative MR fluid; the slope of each dependence is denoted in the legend.

When concerned with 4P models, it can be seen that selected models gave parameters closely correlated to the magnetic field applied. The parameter η for mCA and mCR (including Ex-mCR) models partially followed K values for the HB and RS models, significantly rising upon application of the magnetic field, although the resulting value exhibited unspecific on-state progression. The time constants λ and α generally decreased in line with increase in such a field. These observations could explain the heightened field-induced stiffness of the particle chain structures. The on-state values for the dimensionless N and m parameters of the mCA and both mCR models were almost constant within all the magnetic fields, mimicking the trend of parameter n as observed for the $3P$ models. Conversely, the off-state N and m values were close-to-zero, which is opposed to the typical n value for Newtonian fluids. For the SM model, apart from the τ_0 which demonstrated the behaviour expected, irregular trends were discerned for its K, m, n constants. Thus, it is possible to state that the fitting parameters served primarily as empirical constants for adjustment of the curves. Finally, b parameter in the NA model exhibited non-zero positive values at the off-state and at low magnetic field, while at higher fields (above 144 kA m^{-1}), its value diminished transforming the NA model into the HB model modified with the logarithmic correction term $\ln(1 + \dot{\gamma})$. Parameter k and exponent $(n - m)$ in the NA model were reported to have no physical meaning, and thus, they can get either a positive of negative values (**Nasiri** and **Ash-rafizadeh**, **2010**). Herein, k parameter was generally increasing with magnetic field, until it reached nearly a constant value (above 144 kA m^{-1}). Such field-dependent behaviour was detected also for $(n - m)$ term that changed its values from negative to positive ones (**Table 3**).

3.3. Ranking of models

Comparison of the fitting performance expressed as $RMSE$ of the conventional $3P$ models (**Table S1**) and $4P$ models (**Table 3**) is graphically presented in **Fig. 4**. Generally, the presented models provided acceptable fitting performance superior to that reported previously. For instance (**Chaudhuri et al.**, **2006**), showed that the HB model produced almost 4-fold lower absolute error than the Bingham Plastic model ($2P$). Further enhancements were made herein subsequently as to fitting accuracy.

Overall, the MB model produced the highest values for median and mean RMSE, hence it was deemed the least favourable for describing the data gathered, despite the relatively high R^2 values obtained. The HB model offered slightly better accuracy and its median $RMSE$ was lower by 18%. The RS model proved to have the best fitting accuracy of the $3P$ models, since its median RMSE decreased by an additional 36% compared to HB model, while also exhibiting the lowest interquartile range (IQR) and position of the upper extreme.

As for the $4P$ models, the both mCR and mCA equations clearly converged to the data with fewer deviations over the entire range of shear rate, exceeding the performance of $3P$ ones. Findings for the $RMSE$ of the $4P$ models reinforce the observations discussed in **Section 3.1**. More specifically, as illustrated in **Fig. 4**, the mCR model provided a boxplot with slightly reduced IQR, a lower position of the upper extreme and a similar mean $RMSE$ compared to its mCA analogue. The mCA model, however, exhibited a lower median $RMSE$ (by 11%), suggesting its superior performance. By way of explanation of such a contradiction, it is possible to discern that the mCA model dominated in terms of absolute $RMSE$ (**Table 3**) (four of the most favourable $RMSE$ predictions out of 6 entries); yet it failed to fit the flow curve collected under the highest magnetic field strength. The most suitable option in general was represented by the Ex-mCR model that provided the both, the lowest mean and the lowest median $RMSE$. It is however important to mention that the successful application of the Ex-mCR requires an explicit knowledge of for the investigated MR suspension. The SM model provided relatively good precision and reasonably high R^2, although it was less applicable interestingly than the

RS model ($3P$) and the other $4P$ analogues. This could be attributed to its lower capability to adhere to MR data at a high region of shear rate. The NA model exceeded the performance of the $3P$ models, since the logarithmic correction term ln($1 + \dot{y}$) facilitates fitting of the data in low-shear rate region, and its slope does not approach the infinity at zero $\dot{y}$, in contrast to the HB model (**Nasiri** and **Ashrafizadeh**, **2010**). Compared to the $4P$ equations, mCA and both mCR models were however more suitable in overall predicting behaviour of the MR suspensions

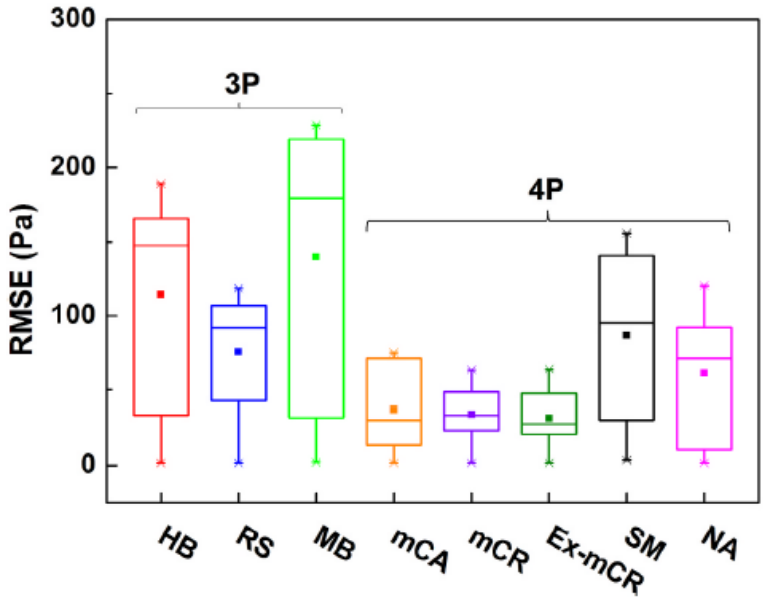

Fig. 4. Boxplot for comparison of RMSE as an output from the tested rheological models (10 points per decade); whiskers are plotted at the maximum and minimum values for each distribution; mean RMSE values are displayed as solid squares.

3.4. Robustness of models, settings of rheometer

It is necessary to emphasize that the relevancy of the fitting models should not be restricted to a narrow class of experimental data (**David et al., 2013b**). A robust rheological model ought to be applicable to a range of MR formulations, including semi-diluted and highly-filled systems operating under different conditions (the intensity of magnetic field perpendicular to the flow, temperature and so on). As reported previously (**Cvek et al.**, **2016**), the ranking of the rheological models in their fitting performance was not markedly affected by the concentrations of the tested MR suspensions. Therefore, this study focussed on investigating other factors that might determine the robustness of the viscoplastic models applied.

The MR suspensions belong to a class of time-dependent complex fluids (**de Vicente** and **Berli, 2013**). The response of such materials can be affected by the measurement protocol, possibly leading to variation in the fitting performance of the corresponding models. For this very reason the settings of the rheometer were altered to assess the robustness of the examined models. In brief, the MR data of the same suspension was collected using either 10 (as above) or 5 data points per decade, giving rise to flow curves differing in data distribution. **Fig. 5** shows the representative flow curve recorded with adherence to the latter protocol.

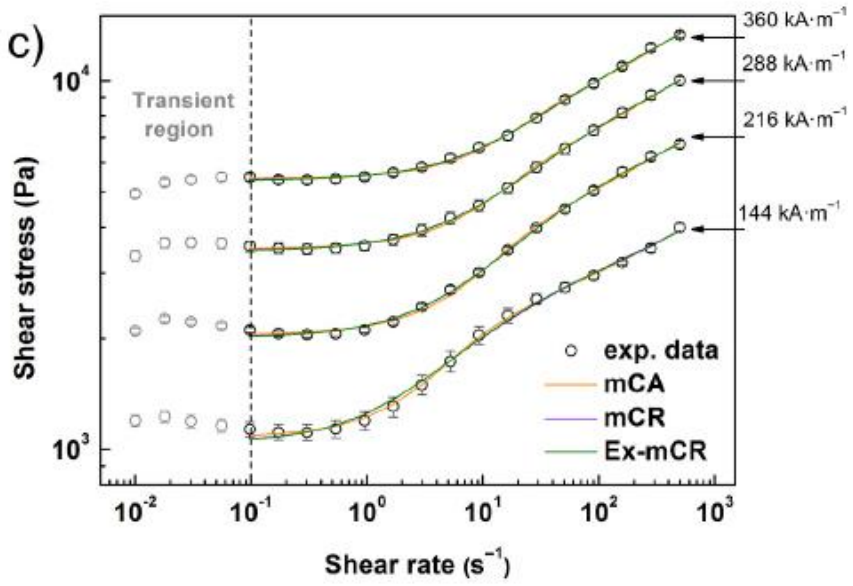

Fig. 5. Shear stress plotted against shear rate for the representative MR fluid (20 pts., Δt = 10 s) under various magnetic field strengths; for clarity, the data was fitted using the mCA, mCR and Ex-mCR models which demonstrated the greatest accuracy; the rest of the graphical results is given in **Fig. S2**.

Although the data points therein were sparsely distributed, the investigated models generally exhibited a satisfactory fitting performance. A complete overview of graphical results is included in the supplementary material, **Fig. S2**. Among the $3P$ models, the RS equation was the most accurate, with its prediction within the error bars. Slight improvement in the fitting accuracy was found upon the application of the NA model ($4P$), while the mCA and both mCR models ($4P$) produced almost identical predictions with exceptional accuracy (**Fig. 5**). In contrast, the HB, MB and SM models were considered the least favourable, since they unambiguously overestimated the data at a high region of shear rate.

The evolution of the fitting parameters with magnetic field for the mCA, mCR and Ex-mCR models is displayed in **Fig. 6**. As seen, the parameters followed similar trends as observed for the protocol (50 pts., Δt = 10 s), **Table 3**. The viscosity parameters, η_∞, η_P and η_0 increased with magnetic field and remained in the range of 112.3 Pa s $< \eta_\infty <$ 121.4 Pa s, 156.1 Pa s $<$ nP $<$ 166.3 Pa s and 175.5 Pa s $< \eta_0 <$ 212.0 Pa s above 200 kA m^{-1}. The time parameters, λ, α, were progressively decreasing with the field, as a result of heightened toughness of the particle chains. The on-state dimensionless parameters, N, m, were nearly constant $0.319 < N < 0.381$, $0.667 < m < 0.810$ for the mCR, and $0.756 < m < 0.879$ for the Ex-mCR, in this way indicating the pseudoplasticity. Based on the data, it appears that the mCA model could be perceived as the favourable option due to the least scatter in the parameter values (**Ezure et al., 2021**).

Next, the overall fitting performance of tested models was compared for datasets obtained using the modified measuring protocol. As seen in **Fig. 7**, general trends in $RMSE$ boxplots were similar with those extracted from the data collected using different rheometer settings. The numerical results are included in **Table S2**. At this point, it should be highlighted that the RS model was quite flexible for accommodating different layout of raw data points, and was proved to be the most suitable $3P$ model. More importantly, the mCA and mCR models ($4P$) provided lower IQR of $RMSE$ and thus superior fitting performance, which was attributed to additional fitting parameters. Between these two models, the mCR provided slightly lower IQR, but higher median $RMSE$, while the difference in the average $RMSE$ value was only marginal (less than 5%). Interestingly, extending the mCR model with the

Quemada equation allowed to predict τ_0 values with even lower error; and the $RMSE$ results from the Ex-mCR model exhibited the lowest IQR, the lowest median and also the average values. Regardless the distribution of the data points (**Fig. 4** vs. **Fig. 7**), the mCA model and both variants of the mCR model clearly offered a well-suited robust assessment of the rheological data, which reflects the suitability of their mathematical structure.

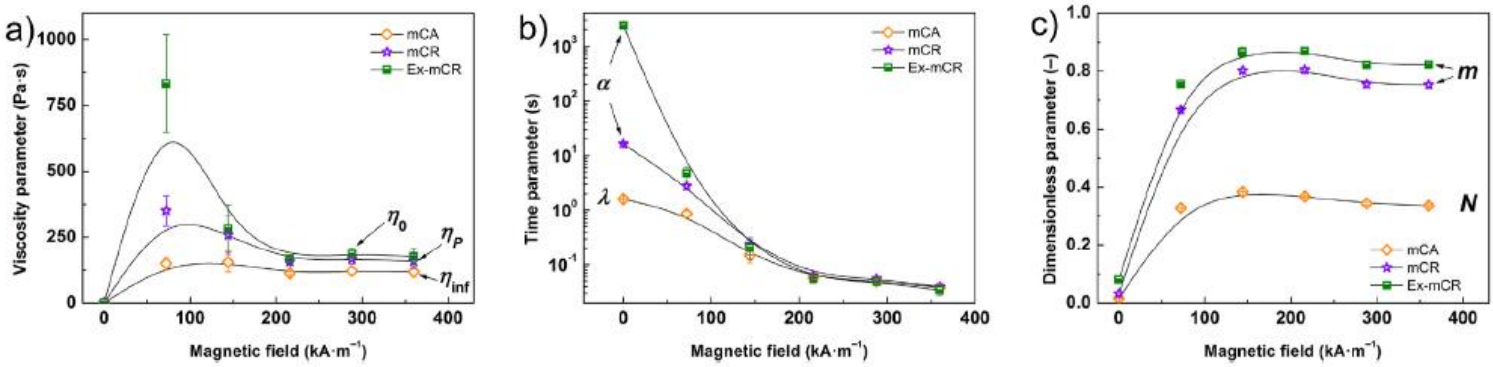

Fig. 6. The fitting parameters for the mCA, mCR and Ex-mCR models (20 pts., $\Delta t = 10$ s) as a function of magnetic field strength. The solid lines represent the B-spline curves.

Taking HB model as a reference, certain improvements (but not as remarkable as in the case of the mCA and both mCR models) were achieved also by using the NA model, which was attributed to its hybrid mathematical structure. On the contrary, the HB, MB and SM models were considered to be insufficient as they exhibited up to 8-times larger IQR of the $RMSE$ values, when compared to the Ex-mCR model. Moreover, they provided up to 4-fold higher average $RMSE$ proving their low fitting capabilities, which was rather unexpected specifically for the SM model that showed low flexibility, especially at the transition to low-ý plateau state (**Fig. S2**c). To conclude, the results demonstrate that the implementation of certain $4P$ models is a reasonable strategy for improving the fitting accuracy in modelling the MR steady shear data.

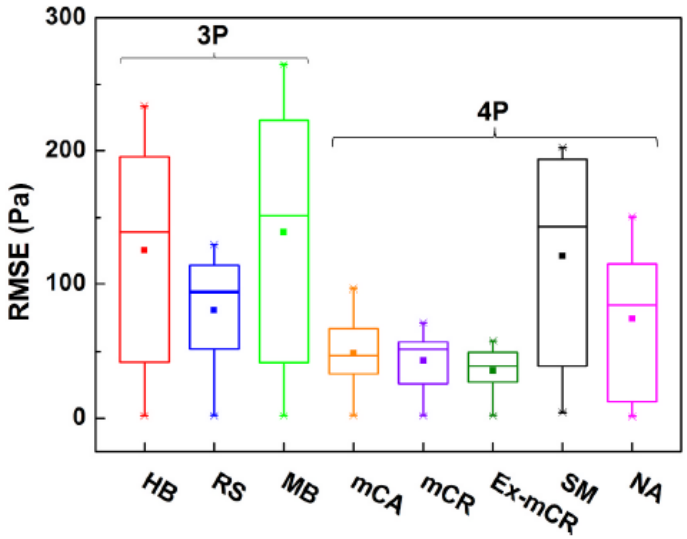

Fig. 7. Boxplot of $RMSE$ comparison as an output from tested rheological models (5 points per decade); whiskers are plotted at the maximum and minimum values for each distribution; mean $RMSE$ values are displayed as solid squares.

4. Conclusions

The presented work endeavours to capture historical development of parametric modelling in shear magnetorheology. The classical $3P$ models were summarized and their applicability to describe flow behaviour of typical MR suspension was confronted with newly implemented $4P$ analogues, namely, mCA, mCR, Ex-mCR, SM and NA models. All models provided acceptable fitting capabilities (high R^2 values), however $3P$ models tend to fail at high shear rate region. The RS model was the most suitable option among $3P$ models, but its fitting capabilities were remarkably surpassed with the $4P$ variants, such as mCA, mCR and Ex-mCR models that exhibited markedly lower $RMSE$ coefficients. All models provided dynamic τ_0 scaling as $\propto H^{1,58\text{-}1,72}$ with differences in t_0 predictions below 15% in absolute values. The values of fitting parameters in the $4P$ models were closely related to applied magnetic field; following the field, the n term values in the mCA and both mCR models generally showed a similar trait as K values in the HB and RS models, with simultaneous decrease in time constants, λ and α. Apart from the off-state situation, their dimensionless N and m parameters were mimicking the trend of n parameter observed in $3P$ models. Somewhat field-dependent trends of b, k and $(n - m)$ were found also in the NA model, but not in the SM model whose parameter values changed rather arbitrarily. The statistical analysis revealed that the mCA and mCR models are robust and provide several-times lower IQR of the $RMSE$ values when compared to their $3P$ analogues. Despite complex interpretation of the parameters, $4P$ models - namely the mCA, mCR and Ex-mCR - were able to provide highly reliable and robust description of the rheological data, regardless the distribution of the data points as an input given by the operator. The obtained results are of practical relevance for the design of hydraulic MR smart devices, in which the flow field of the MR fluid and the internal characteristics can be obtained by injecting an appropriate rheological equation into a fluid dynamic solver. The open question remains whether some analogy in improving fitting accuracy exists in other viscoplastic systems, e.g. food, cosmetic and pharmaceutical products, polymer solutions, drilling fluids, cement mixtures, asphalts, propellants, among the others.

References

Datasheet data. ARUS MR tech. Available online: **https://amsmrtech.com** (accessed on February, 2022).

Datasheetb. LORD corporation. Available online: **https://lord.com** (accessed on February, 2022).

Andaverde, J.A., Wong-Loya, J.A., Vargas-Tabares, Y., Robles, M., 2019. A practical method for determining the rheology of drilling fluid. J. Pet. Sci. Eng. 180, 150-158. **https://doi.org/10.1016/j.petrol.2019.05.039**.

Apostolidis, A.J., Beris, A.N., 2014. Modeling of the blood rheology in steady-state shear flows. J. Rheol. 58, 607-633. **https://doi.org/10.1122/1.4866296**.

Bahiuddin, I., Mazlan, S.A., Shapiai, I., Imaduddin, F., Ubaidillah, Choi, S.B., 2018a. Constitutive models of magnetorheological fluids having temperature-dependent prediction parameter. Smart Mater. Struct. 27, 095001 **https://doi.org/10.1088/ 1361-665X/aac237**.

Bahiuddin, I., Mazlan, S.A., Shapiai, M.I., Choi, S.B., Imaduddin, F., Rahman, M.A.A., Ariff, M.H.M., 2018b. A new constitutive model of a magneto-rheological fluid actuator using an extreme learning machine method. Sens. Actuators, A 281, 209-221. **https://doi.org/10.1016/j.sna.2018.09.010**.

Bahiuddin, I., Mazlan, S.A., Shapiai, M.I., Imaduddin, F., Ubaidillah, Choi, S.B., 2019. A new platform for the prediction of field-dependent yield stress and plastic viscosity of magnetorheological fluids using particle swarm optimization. Appl. Soft Comput. 76, 615-628. **https://doi.org/10.1016/j.asoc.2018.12.038**.

Baldino, S., Osgouei, R.E., Ozbayoglu, E., Miska, S.Z., May, R., 2018. Quemada model approach to oil or synthetic oil based drilling fluids rheological modelling. J. Pet. Sci. Eng. 163, 27-36. **https://doi.org/10.1016/j.petrol.2017.12.042**.

Barnes, H.A., 1999. The yield stress - a review or 'pi alpha nu tau alpha rho epsilon iota' -everything flows? J. Non-Newtonian Fluid Mech. 81, 133-178. **https://doi.org/ 10.1016/s0377-0257(98)00094-9**.

Bossis, G., Lacis, S., Meunier, A., Volkova, O., 2002a. Magnetorheological fluids. J. Magn. Magn Mater. 252, 224-228. **https://doi.org/10.1016/s0304-8853(02)00680-7**.

Bossis, G., Volkova, O., Lacis, S., Meunier, A., 2002b. Magnetorheology: fluids, structures and rheology. In: Odenbach, S. (Ed.), Ferrofluids: Magnetically Controllable Fluids and Their Applications. Springer Berlin Heidelberg, Berlin, Heidelberg, pp. 202-230. **https://doi.org/10.1007/3-540-45646-5_11**.

Carrier, V., Petekidis, G., 2009. Nonlinear rheology of colloidal glasses of soft thermosensitive microgel particles. J. Rheol. 53, 245-273. **https://doi.org/10.1122/I.3045803**.

Chaudhuri, A., Wereley, N.M., Radhakrishnan, R., Choi, S.B., 2006. Rheological parameter estimation for a ferrous nanoparticle-based magnetorheological fluid using genetic algorithms. J. Intell. Mater. Syst. Struct. 17, 261-269. **https://doi.org/10.1177/1045389x06063038**.

Cvek, M., Mrlik, M., Pavlinek, V., 2016. A rheological evaluation of steady shear magnetorheological flow behavior using three-parameter viscoplastic models. J. Rheol. 60, 687-694. **https://doi.org/10.1122/1.4954249**.

Cvek, M., Mrlik, M., Moucka, R., Sedlacik, M., 2018. A systematical study of the overall influence of carbon allotrope additives on performance, stability and redispersibility of magnetorheological fluids. Colloids Surf., A 543, 83-92. **https://doi.org/10.1016/ j.colsurfa.2018.01.046**.

Cvek, M., Torres-Mendieta, R., Havelka, O., Urbanek, M., Plachy, T., Cernik, M., 2020. Laser-induced fragmentation of carbonyl iron as a clean method to enhance magnetorheological effect. J. Clean. Prod. 254, 120182 **https://doi.org/10.1016/). jclepro.2020.120182**.

Cvek, M., Kollar, J., Mrlik, M., Masar, M., Suly, P., Urbanek, M., Mosnacek, J., 2021. Surface-initiated mechano-ATRP as a convenient tool for tuning of bidisperse magnetorheological suspensions toward extreme kinetic stability. Polym. Chem. 12, 5093-5105. **https://doi.org/10.1039/d1py00930c**.

Daniel, G., Yoan, C., Zoltan, P., Yves, P., 2014. Bingham-Papanastasiou and approximate parallel models comparison for the design of magneto-rheological valves. IEEE/ ASME Int. Conf. Adv. Intell. Mechatronics (AIM). Ieee, Besancon, France 168-173.

David, J., Filip, P., Kharlamov, A.A., 2013a. Back extrusion of Vocadlo-type fluids. Appl. Rheol. 23, 45366 **https://doi.org/10.3933/ApplRheol-23-45366**.

David, J., Filip, P., Kharlamov, A.A., 2013b. Empirical modelling of nonmonotonous behaviour of shear viscosity. Adv. Mater. Sci. Eng. 658187 **https://doi.org/10.1155/ 2013/658187**.

de Vicente, J., Berli, C.L.A., 2013. Aging, rejuvenation, and thixotropy in yielding magnetorheological fluids. Rheol. Acta 52, 467-483. **https://doi.org/10.1007/ s00397-013-0704-8**.

de Vicente, J., Klingenberg, D.J., Hidalgo-Alvarez, R., 2011. Magnetorheological fluids: a review. Soft Matter 7, 3701-3710. **https://doi.org/10.1039/c0sm01221a**.

Divoux, T., Barentin, C., Manneville, S., 2011. Stress overshoot in a simple yield stress fluid: an extensive study combining rheology and velocimetry. Soft Matter 7, 9335-9349. **https://doi.org/10.1039/c1sm05740e**.

Divoux, T., Fardin, M.A., Manneville, S., Lerouge, S., 2016. Shear banding of complex fluids. Annu. Rev. Fluid Mech. 48, 81-103. **https://doi.org/10.1146/annurev-fluid-122414-034416**.

Elsaady, W., Oyadiji, S.O., Nasser, A., 2020. A one-way coupled numerical magnetic field and CFD simulation of viscoplastic compressible fluids in MR dampers. Int. J. Mech. Sci. 167, 105265 **https://doi.org/10.1016/j.ijmecsi.2019.105265**.

Esmaeilnezhad, E., Choi, H.J., Schaffie, M., Gholizadeh, M., Ranjbar, M., Kwon, S.H., 2017. Rheological analysis of magnetite added carbonyl iron based magnetorheological fluid. J. Magn. Magn Mater. 444, 161-167. **https://doi.org/ 10.1016/j.jmmm.2017.08.023**.

Ezure, R., Sagawa, T., Horiguchi, T., Arai, Y., Komatsu, H., Yamagiwa, K., Tajima, H., 2021. Flow characteristics of hydrofluorocarbon gas hydrate slurries under various conditions in a loop tube. Chem. Eng. Sci. 246, 116974 **https://doi.org/10.1016/j. ces.2021.116974**.

Farjoud, A., Ahmadian, M., Mahmoodi, N., Zhang, X., Craft, M., 2011. Nonlinear modeling and testing of magneto-rheological fluids in low shear rate squeezing flows. Smart Mater. Struct. 20, 085013 **https://doi.org/10.1088/0964-1726/20/8Z 085013**.

Gao, C.Y., Kim, M.W., Bae, D.H., Dong, Y.Z., Piao, S.H., Choi, H.J., 2017. Fe3O4 nanoparticle-embedded polystyrene composite particles fabricated via a Shirasu porous glass membrane technique and their magnetorheology. Polymer 125, 21-29. **https://doi.org/10.1016/j.polymer.2017.07.079**.

Ginder, J.M., Davis, L.C., Elie, L.D., 1996. Rheology of magnetorheological fluids: models and measurements. Int. J. Mod. Phys. B 10, 3293-3303. **https://doi.org/10.1142/ s0217979296001744**.

Gorislavec, V.M., Smol'skii, B.M., Shul'man, Z.P., 1968. Rheophysics and Rheodynamics, Nauka i technika ed. (in Russian) Minsk.

Gullu, H., 2016. Comparison of rheological models for jet grout cement mixtures with various stabilizers. Construct. Build. Mater. 127, 220-236. **https://doi.org/10.1016/ j.conbuildmat.2016.09.129**.

Hodne, H., Galta, S., Saasen, A., 2007. Rheological modelling of cementitious materials using the Quemada model. Cement Concr. Res. 37, 543-550. **https://doi.org/ 10.1016/j.cemconres.2006.11.020**.

Jonkkari, I., Syrjala, S., 2011. Transient rheology of a magnetorheological fluid under shearing. Annu. Trans. - Nord. Rheol. Soc. 19.

Jonkkari, I., Kostamo, E., Kostamo, J., Syrjala, S., Pietola, M., 2012. Effect of the plate surface characteristics and gap height on yield stresses of a magnetorheological fluid. Smart Mater. Struct. 21, 075030 **https://doi.org/10.1088/0964-1726/21/7/ 075030**.

Kelessidis, V.C., Maglione, R., 2006. Modeling rheological behavior of bentonite suspensions as Casson and Robertson-Stiff fluids using Newtonian and true shear rates in Couette viscometry. Powder Technol. 168, 134-147. **https://doi.org/ 10.1016/j.powtec.2006.07.011**.

Khan, M., Sardar, H., Gulzar, M.M., Alshomrani, A.S., 2018. On multiple solutions of non-Newtonian Carreau fluid flow over an inclined shrinking sheet. Results Phys. 8, 926-932. **https://doi.org/10.1016/j.rinp.2018.01.021**.

Knutsen, S., Cayeux, E., Saasen, A., Khalifeh, M., 2021. Application of the Quemada Viscosity model for drilling fluids. In: Proc. ASME 2021 Int. Conf. Ocean, Offshore Arct. Eng., 40th. **https://doi.org/10.1115/OMAE2021-60500**.

Kuzhir, P., Bossis, G., Bashtovoi, V., Vekas, L., 2005. Capillary flow of a suspension of non-magnetic particles in a ferrofluid under highly non-uniform magnetic field. Int. J. Multiphas. Flow 31, 201-221. **https://doi.org/10.1016/j. ijmultiphaseflow.2004.09.006**.

Laun, H.M., Gabriel, C., Kieburg, C., 2011. Wall material and roughness effects on transmittable shear stresses of magnetorheological fluids in plate-plate magnetorheometry. Rheol. Acta 50, 141-157. **https://doi.org/10.1007/s00397-011-0531-8**.

Mannarswamy, A., Munson-McGee, S.H., Andersen, P.K., 2010. D-optimal designs for the Cross viscosity model applied to guar gum mixtures. J. Food Eng. 97, 403-409. **https://doi.org/10.1016/j.jfoodeng.2009.10.035**.

Min, T.H., Choi, H.J., Kim, N.H., Park, K., You, C.Y., 2017. Effects of surface treatment on magnetic carbonyl iron/polyaniline microspheres and their magnetorheological study. Colloids Surf., A 531, 48-55. **https://doi.org/10.1016/j. colsurfa.2017.07.070**.

Mohamed, A., Salehi, S., Ahmed, R., 2021. Significance and complications of drilling fluid rheology in geothermal drilling: a review. Geothermics 93, 102066. **https:// doi.org/10.1016/j.geothermics.2021.102066**.

Nasiri, M., Ashrafizadeh, S.N., 2010. Novel equation for the prediction of rheological parameters of drilling fluids in an annulus. Ind. Eng. Chem. Res. 49, 3374-3385. **https://doi.org/10.1021/ie9009233**.

Papanastasiou, T.C., 1987. Flows of materials with yield. J. Rheol. 31, 385-404. **https:// doi.org/10.1122/1.549926**.

Pease, L.F., Daniel, R.C., Burns, C.A., 2019. Slurry rheology of Hanford sludge. Chem. Eng. Sci. 199, 628-634. **https://doi.org/10.1016/j.ces.2018.12.044**.

Pelegrine, D.H., Silva, F.C., Gasparetto, C.A., 2002. Rheological behavior of pineapple and mango pulps. Food Sci. Technol. 35, 645-648. **https://doi.org/10.1006/fstl.2002.0920**.

Pivokonsky, R., Filip, P., 2014. Predictive/fitting capabilities of differential constitutive models for polymer melts-reduction of nonlinear parameters in the eXtended PomPom model. Colloid Polym. Sci. 292, 2753-2763. **https://doi.org/10.1007/s00396-014-3308-7**.

Plachy, T., Kutalkova, E., Sedlacik, M., Vesel, A., Masar, M., Kuritka, I., 2018. Impact of corrosion process of carbonyl iron particles on magnetorheological behavior of their suspensions. J. Ind. Eng. Chem. 66, 362-369. **https://doi.org/10.1016/j.jiec.2018.06.002**.

Poslinski, A.J., Ryan, M.E., Gupta, R.K., Seshadri, S.G., Frechette, F.J., 1988. Rheological behavior of filled polymeric systems I. Yield stress and shear-thinning effects. J. Rheol. 32, 703-735. **https://doi.org/10.1122/1.549987**.

Quemada, D., 1998. Rheological modelling of complex fluids. I. The concept of effective volume fraction revisited. Eur. Phys. J. Appl. Phys. 1, 119-127. **https://doi.org/ 10.1051/epjap:1998125**.

Rabinow, J., 1948. The magnetic fluid clutch. AIEE Trans 67, 1308-1315. **https://doi.org/10.1109/T-AIEE.1948.5059821**.

Rayment, P., RossMurphy, S.B., Ellis, P.R., 1995. Rheological properties of guar galactomannan and rice starch mixtures: 1. Steady shear measurements. Carbohydr. Polym. 28, 121-130. **https://doi.org/10.1016/0144-8617(95)00110-7**.

Rayment, P., Ellis, P.R., Ross-Murphy, S.B., 2000. Rheological Properties of Guar Galactomannan Solutions Filled with Particulate Inclusions. Elsevier Science Bv, Amsterdam, pp. 193-198.

Romano, M.R., Cuomo, F., Massarotti, N., Mauro, A., Salahudeen, M., Costagliola, C., Ambrosone, L., 2017. Temperature effect on rheological behavior of silicone oils: a model for the viscous heating. J. Phys. Chem. B 121, 7048-7054. **https://doi.org/ 10.1021/acs.jpcb.7b03351**.

Ronzova, A., Sedlacik, M., Cvek, M., 2021. Magnetorheological fluids based on core-shell carbonyl iron particles modified by various organosilanes: synthesis, stability and performance. Soft Matter 17, 1299-1306. **https://doi.org/10.1039/d0sm01785j**.

Roupec, J., Jenis, F., Strecker, Z., Kubik, M., Machacek, O., 2020. Stribeck curve of magnetorheological fluid within pin-on-disc configuration: an experimental investigation. Materials 13, 4670. **https://doi.org/10.3390/ma13204670**.

Ruiz-Lopez, J.A., Fernandez-Toledano, J.C., Hidalgo-Alvarez, R., de Vicente, J., 2016. Testing the mean magnetization approximation, dimensionless and scaling numbers in magnetorheology. Soft Matter 12, 1468-1476. **https://doi.org/10.1039/ c5sm02267c**.

Ruiz-Lopez, J.A., Hidalgo-Alvarez, R., de Vicente, J., 2017. Towards a universal master curve in magnetorheology. Smart Mater. Struct. 26, 054001 **https://doi.org/10.1088/1361-665X/aa6648**.

Skadsem, H.J., Saasen, A., 2019. Concentric cylinder viscometer flows of Herschel-Bulkley fluids. Appl. Rheol. 29, 173-181. **https://doi.org/10.1515/arh-2019-0015**.

Song, K.W., Kim, Y.S., Chang, G.S., 2006. Rheology of concentrated xanthan gum solutions: steady shear flow behavior. Fibers Polym. 7, 129-138. **https://doi.org/ 10.1007/bf02908257**.

Susan-Resiga, D., 2009. A rheological model for magneto-rheological fluids. J. Intell. Mater. Syst. Struct. 20, 1001-1010. **https://doi.org/10.1177/1045389X08100979**.

Tao, R., 2001. Super-strong magnetorheological fluids. J. Phys. Condens. Matter 13, R979-R999. **https://doi.org/10.1088/0953-8984/13/50/202**.

Ulicny, J.C., Golden, M.A., Namuduri, C.S., Klingenberg, D.J., 2005. Transient response of magnetorheological fluids: shear flow between concentric cylinders. J. Rheol. 49, 87-104. **https://doi.org/10.1122Z1.1803576**.

Volkova, O., Cutillas, S., Bossis, G., 1999. Shear banded flows and nematic-to-isotropic transition in ER and MR fluids. Phys. Rev. Lett. 82, 233-236. **https://doi.org/ 10.1103/PhysRevLett.82.233**.

Wang, Z., Shahrivar, K., de Vicente, J., 2014. Creep and recovery of magnetorheological fluids: experiments and simulations. J. Rheol. 58, 1725-1750. **https://doi.org/ 10.1122/1.4891247**.

Wollny, K., Lauger, J., Huck, S., 2001. Magneto sweep - a new method for characterizing the viscoelastic properties of magneto-rheological fluids. Appl. Rheol. 12, 25-31. **https://doi.org/10.1515/arh-2002-0003**.